

Analysis of wavefront effects for large-aperture tiled-grating compressor

S. Zhang^{1,2}, J. W. Zhang², Y. Zhou¹, J. Q. Su², X. Wang², B. Deng² and D. X. Hu²

¹College of Mechanical Engineering, Chongqing University, Chongqing, China and ²Research Center of Laser Fusion, China Academy of Engineering Physics, Mianyang, Sichuan, China

Original Study

Cite this article: Zhang S, Zhang JW, Zhou Y, Su JQ, Wang X, Deng B, Hu DX (2018). Analysis of wavefront effects for large-aperture tiled-grating compressor. *Laser and Particle Beams* **36**, 84–91. <https://doi.org/10.1017/S0263034617000878>

Received: 9 October 2017
Accepted: 14 November 2017

Key words:

Pulse compression; systems design; tiled gratings; ultrafast lasers; wavefront error

Author for correspondence:

J. W. Zhang, Research Center of Laser Fusion, China Academy of Engineering Physics, Mianyang, Sichuan, China.
E-mail: zhangjunwei@caep.ac.cn

Abstract

Monolithic large-aperture diffraction grating tiling is desired to increase the output capability of multi-kilojoule petawatt laser facilities. However, the wavefront errors of input pulse and gratings will degrade the focal spot quality and the compressibility of the output pulse. In this work, the effects of wavefront error of input pulse, deformation and wave aberration of the grating for the large-aperture tiled-grating compressor are investigated theoretically. A series of numerical simulations are presented to discuss the changing trends of focal spot energy caused by wavefront error of input pulse and obtain the error tolerance for specific goals. The influences of coating stress and the wave aberration of holographic exposure gratings on the diffraction wavefront are also discussed. Some advice is proposed for improving the performance of large-aperture tiled-grating. This work paves the way for the design of practical large-aperture tiled-grating compressor for ultrahigh intensity laser facilities in the future.

Introduction

The well-known technique of Chirped Pulse Amplification (CPA) is used to construct high-energy petawatt (HEPW) laser systems at worldwide laboratories (Bunkenburg *et al.*, 2006; Mourou & Tajima, 2011; Dorrer *et al.*, 2015). In CPA laser systems, large-aperture diffraction gratings are necessary components to recompress pulses to provide the ultrahigh on-target optical intensity (Jahns *et al.*, 1999; Kessler *et al.*, 2004; Qiao *et al.*, 2007; Yakovlev, 2014). Holographic gratings formed from a combination of a multi-layer dielectric (MLD) are highly desired pulse compression element for their high laser damage threshold and high diffraction efficiency (Oliver *et al.*, 2005; Smith *et al.*, 2008; Yakovlev, 2014; Bonod & Neauport, 2016). The fluence damage threshold of gratings is one of the limitations on increasing the output capability of systems, and expanding the aperture of gratings can enable the construction of the laser systems providing higher on-target energy (Yakovlev, 2014; Bonod & Neauport, 2016). The size available for monolithic gratings does not exceed 1 meter, which makes grating tiling as an alternative solution to meet the aperture demand of compressor (Zhang *et al.*, 1998; Kessler *et al.*, 2004; Qiao *et al.*, 2007).

The grating tiling technique (GTT) has been implemented in several laser systems in the past decade (Qiao *et al.*, 2007; Blanchot *et al.*, 2010; Habara *et al.*, 2010). Many theoretical and experimental studies have been performed to limit tiling errors of large-aperture tiled-grating (LATG) within the error tolerances (Bunkenburg *et al.*, 2006; Qiao *et al.*, 2007; Zuo *et al.*, 2007; Li *et al.*, 2010; Daiya *et al.*, 2013, 2017; Fang *et al.*, 2014; Sharma *et al.*, 2017). Most of them base on far-field focal spot image or near-field interference fringe pattern. However, Qiao *et al.* observe that the far field image has multiple split spots even if there are no tiling errors when conducting LATG, and they point out that the wavefront is another key factor for LATG (Qiao *et al.*, 2007). Many factors can cause the wavefront distortion and decrease the focal spot quality. Firstly, the LATGs should be placed in a high-vacuum environment to avoid the dispersion and the nonlinear effect of the air, but the stresses between coatings and substrates of MLD grating will change in ambient atmospheric and high-vacuum environment. The magnitude of the stresses is high enough to cause significant deformation of the diffracted wavefront (Oliver *et al.*, 2005; Smith *et al.*, 2008). In some systems, the large-aperture deformable mirror is used to correct the LATG wavefront error (Kruschwitz *et al.*, 2006). Interestingly, Qiao *et al.* propose the idea of the large-aperture deformable grating to decrease the deformation of the grating (Qiao *et al.*, 2015) and Reinlein *et al.* have proved the feasibility of deformable grating experimentally (Reinlein *et al.*, 2016). Furthermore, the structures of holographic exposure gratings have smoother shapes with lower roughness, so the MLD gratings processed with holographic exposure are mainly used in CPA systems. However, the wave aberration of these gratings is unavoidable in the fabrication process (Shi *et al.*, 2009; Bonod & Neauport, 2016) and must be well controlled when constructing

the LATG to allow focusing to a small spot on the target. Meanwhile, if the wavefront of the large-size input beam for the compressor is not perfectly flat wavefront, which is subject to disturbance induced by turbulence and vibration, energy could not focused on the focal point well.

Nevertheless, little attention has been focused on the influences of above wavefront errors when constructing the LATG compressor, and the specific impacts of these errors on the performance of LATG are rarely mentioned in the previous works. In this paper, we will theoretically investigate the wavefront effects for LATG compressor on the tiling performance in detail. This research is significant and practical for constructing LATG compressor. This paper is organized as follows. The section “Theoretical model” presents a physical model of tiled-grating (TG). The wavefront error of input pulse (IPWE) is described in the section “Requirement of IPWE for LATG compressor”. The grating wavefront error is raised in the section “Influence of grating wavefront error for LATG compressor”. Discussions are listed in the section “Discussion”. Conclusions are drawn in the section “Conclusion”.

Theoretical model

The multi-pass compressors, which typically use a minimum of four passes on a grating or a series, are applied to provide negative dispersion to compress the input laser pulse. An optical model of the typical two-pass Z-type compressor is illustrated in Figure 1 (Hornung *et al.*, 2010; Yakovlev, 2014). TG G1 and G2 contain two small-aperture gratings each, G11 and G12, G21, and G22, respectively. In such an arrangement, the laser pulse hits the first TG and becomes angular dispersion. It has been broadened in one lateral direction when it hits the second TG, where the wavelengths are distributed over the two tiles. The tilt angle of folding mirror makes the laser pulse tilt down with a small angle to send back to grating tiles. The compressed output laser pulse is focused by an *f*/2 off-axis parabola. Wavefront distribution is an important issue since it markedly decreases the focal spot quality and the compressibility of the output pulse, and must be considered in a model for the TG systems.

The electric field of laser pulse can be expressed as a vector superposition of the electric field of different frequency components, and the electric field expression in the frequency domain

is obtained by Fourier transforming of that in time domain, they can be represented as

$$\begin{aligned} \varepsilon(x, y, t) &= \frac{1}{2\pi} \int_{-\infty}^{\infty} E(x, y, \omega) \exp(-i\omega t) d\omega \\ E(x, y, \omega) &= \int_{-\infty}^{\infty} \varepsilon(x, y, t) \exp(i\omega t) dt \end{aligned} \tag{1}$$

where $\varepsilon(x, y, t)$ shows the time domain expression at spatial coordinate (x, y) , and $E(x, y, \omega)$ is the corresponding frequency domain representation.

Assuming the spatial intensity distribution and time-domain waveform of input pulse in the compressor are independent, and the shape of beam aperture is square. The pulse waveform and the shape of beam aperture can be expressed as

$$\begin{aligned} E_{in}(x, y, \omega) &= A(x, y)E(\omega) \exp(-i\varphi_0(x, y)) \\ A(x, y) &= \exp[-(2x/D)^{2m}] \exp[-(2y/D)^{2m}] \end{aligned} \tag{2}$$

where (x, y) is the coordinate of the near field, $E_{in}(x, y, \omega)$ is the near distribution, $A(x, y)$ is the spatial intensity distribution, $E(\omega)$ is the spectral function, $\varphi_0(x, y)$ is the phase distribution, D is the beam aperture and m is the order of super-Gaussian laser beam.

The compressed pulse at the focal plane of the focusing optic is obtained by principle of Fraunhofer far-field diffraction, which can be expressed as

$$\begin{aligned} E_f(x_f, y_f, \omega) &= C \iint E_{in}(x, y, \omega) \exp[-i\varphi(x, y, \omega)] \\ &\quad \exp\left[-i\frac{\omega}{cf}(x_f x + y_f y)\right] dx dy \end{aligned} \tag{3}$$

where $C = (1/if) \exp(i\omega/cf) \exp[(i\omega/2cf)(x_f^2 + y_f^2)]$ is the coefficient factor, (x_f, y_f) is the coordinate of the focal plane. $\varphi(x, y, \omega)$ is phase obtained by propagating in the compressor and can be calculated by tracing the optical path length at each point (x, y) of the input beam for each frequency component ω . If the sample frequency of point is high enough, the effects of the wavefront error and the light escaping of tiling gap on the tiling

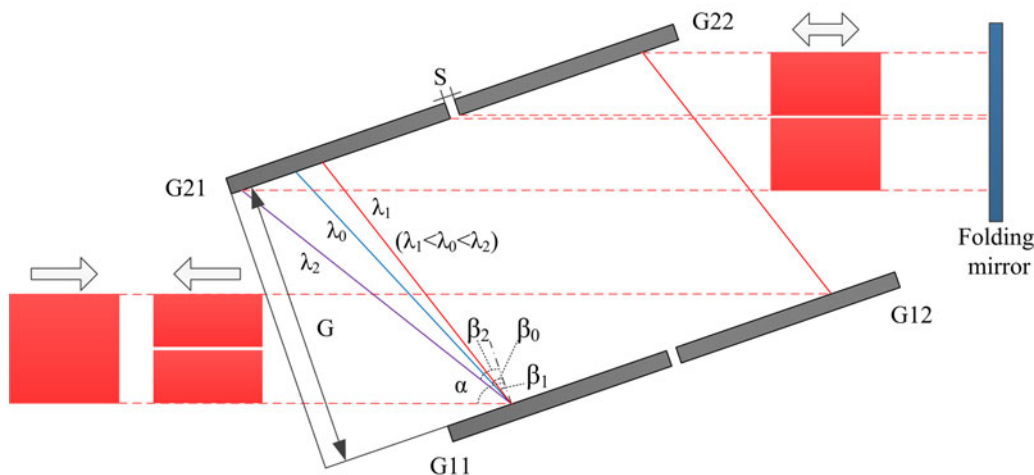


Fig. 1. Optical model of the two-pass Z-type compressor.

Table 1. Simulation parameters of LATG compressor

Parameters of TG compressor		Parameters of input pulse	
Grating period (gr/mm)	1740	Central frequency (nm)	1053
Incident angle α (°)	71	Spectral bandwidth (nm)	3
Perpendicularity distance (m)	1.86	Chirp ratio $\Delta t/\Delta\lambda$ (ps/nm)	400
Grating aperture (mm \times mm)	455 \times 420	Beam aperture (mm \times mm)	285 \times 285
Grating gap (mm)	4	–	–
Tilt angle of M3 (°)	0.45	–	–
Focal distance f (m)	0.8	–	–

performance can be reflected adequately. f is the focal distance of the parabola and c is the velocity of light.

The different spectral components propagate to focal plane independently. The focal spot electric field is the vector superposition of the far field electric field distribution of different spectral components, the intensity of the far field is

$$I_f(x_f, y_f) = \int |E_f(x_f, y_f, \omega)|^2 d\omega \quad (4)$$

The inverse Fourier transform of spectral function of point (x_f, y_f) is time-domain pulse waveform of far field, which can be denoted as

$$E_f(x_f, y_f, t) = \frac{1}{2\pi} \int E_f(x_f, y_f, \omega) \exp(-i\omega t) d\omega \quad (5)$$

To evaluate the performance of LATG, we prefer to use the Strehl ratio (SR) and the power in the bucket (PIB) in the diffraction limit to present peak intensity information and the concentration of energy, respectively. SR is the ratio of peak intensity of an aberrated system to that of an ideal system, and PIB is the ratio of the energy in a certain bucket of far field to the total energy. The peak-to-valley (PV) and the root mean square (RMS) of the wavefront error is used to reflect the influence of the wavefront error on LATG performance. Besides, the root mean square of the gradient (GRMS) of the wavefront error and the peak-to-valley (GPV) of the gradient of the wavefront error are applied to show the property of focusing of the laser beam.

The Nd:glass amplifiers are widely adopted in HEPW laser systems (Dorner *et al.*, 2015). The optical spectrum is narrowed down to ~ 3 nm prior to compression in the TG compressor because of the gain narrowing of the Nd:glass amplifiers. Therefore, a ten order super-Gaussian laser beam centered at 1053 nm with bandwidth 3 nm is used to investigate the wavefront effect in a computer model, which can also take the compressor tiling errors into account. The detail of parameters of the numerical simulation model is listed in Table 1. The SR and PIB for an ideal system in our model are 1 and 0.8475, respectively.

Requirement of IPWE for LATG compressor

For a TG compressor to form a focal spot with 90% of the diffraction-limited energy distribution, the tiling errors X tilt, Y tip and piston cannot exceed a few tens of sub-micro radians and nanometers. However, energy could not be focused on the focal spot even if there is no tiling error. The IPWE decreases the performance of tiling significantly due to the intrinsic nature of coherent beam combination. To explain the physical meaning of our discussion clearer,

the influence of the IPWE on the tiling performance is indicated in Figure 2. Figure 2a and 2b are a perfectly flat input wavefront and the ideal far field, respectively. Figure 2c indicates the far field with the tiling accuracy piston = 75 nm and the flat pulse, piston error could change far field distribution dramatically due to the intrinsic nature of interference and lead to focal spot splitting symmetrically. Figure 2d exhibits a non-flat input wavefront and Figure 2e is the corresponding far field without tiling error. Figure 2f displays the far field with the non-flat input wavefront and the tiling accuracy piston = 75 nm. It is clear that far field intensity distribution degenerates significantly when input pulse's own wavefront error becomes greater. Introducing the same type and same value of tiling error in the compressor, the amount of degradation of far field is clearly greater for a perfectly flat input wavefront than that for a non-flat input wavefront. For the latter case, the IPWE is the major factor that determines the far field quality.

Taking into account the complexity of LATG, the Monte Carlo method is introduced to find out the relationships between IPWE and LATG performance and get the requirements of IPWE. To simulate different IPWEs, a series of random phase screens are generated by (Lawson *et al.*, 1999)

$$\varphi_0(x, y) = k \times \text{random}(-1, 1) \otimes \exp \left\{ - \left[\left(\frac{x}{sg_x} \right)^2 + \left(\frac{y}{sg_y} \right)^2 \right] \right\} \quad (6)$$

where k is the proportionality coefficient, $\text{rand}(-1, 1)$ is a uniform distribution random number sequence in the range of -1 to 1 . \otimes means convolution. sg_x and sg_y are the parameters corresponding to the spatial distribution of low-frequency phase, and the range is 2–12 cm in this paper.

For each value of the wavefront error, SR and PIB are calculated by repeating introduced the IPWE 200 times at each point, and we change the computational interval to increase the correctness of estimation in some simulation. The relationships between parameters (PV, RMS, GPV, and GRMS) of IPWE and SR, PIB are represented in Figure 3a–3d. Statistical means of SR and PIB are given by points and connected by solid lines, and statistical standard deviations are given by error bar. The relationships between IPWE and performance of LATG are obtained by data fitting. Because the energy could not be focused on the focal plane well, SR degrades significantly when the input wavefront degenerates and decreases faster to wavefront error than PIB. The standard deviations of the SR and PIB increase with the increased IPWE, that is the greater IPWE, the greater change range of SR and PIB. Comparing with the subgraphs in Figure 3, we can conclude that the RMS and PV can be better to predict the

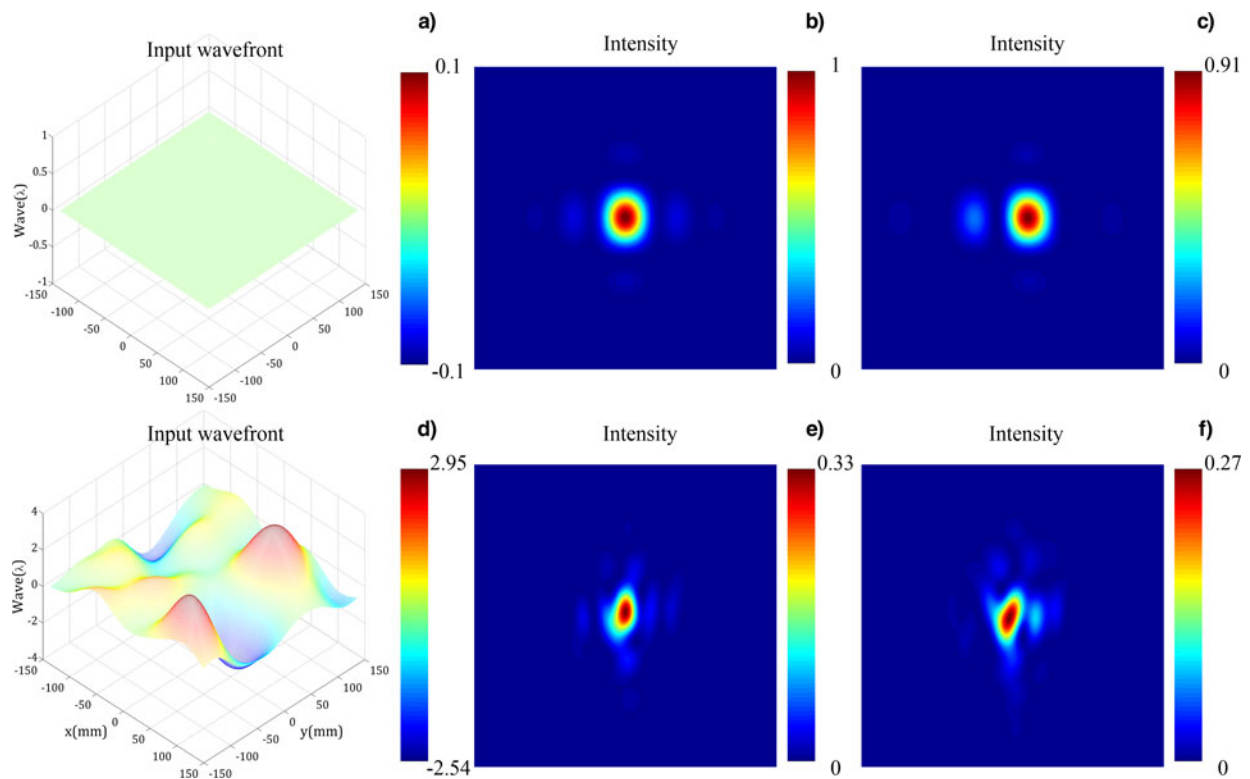


Fig. 2. Input wavefront or the far-field distribution. (a) Perfectly flat input wavefront, (b) ideal far field with flat input wavefront, and (c) far-field with flat input wavefront and piston =75 nm. (d) A non-flat input wavefront, (e) far-field with the non-flat input wavefront, and (f) far-field with non-flat input wavefront and piston =75 nm.

influence of IPWE on SR than GRMS and GPV, and SR decreases divergently with the increased GRMS and GPV. Assuming SR equivalent to 0.9 or PIB equivalent to 0.9 relative to ideal value is used to as the goal, the corresponding wavefront error demands are listed in Table 2. These can be used as a design reference of LATG compressor in the future.

Influence of grating wavefront error for LATG compressor

The grating wavefront error, that is wavefront of the diffracted wave, consists of a mirror term and a holographic term and is an important indicator for diffracted grating. The mirror term refers to the surface deformation caused by substrate gravity, tiled mount, coating stress,

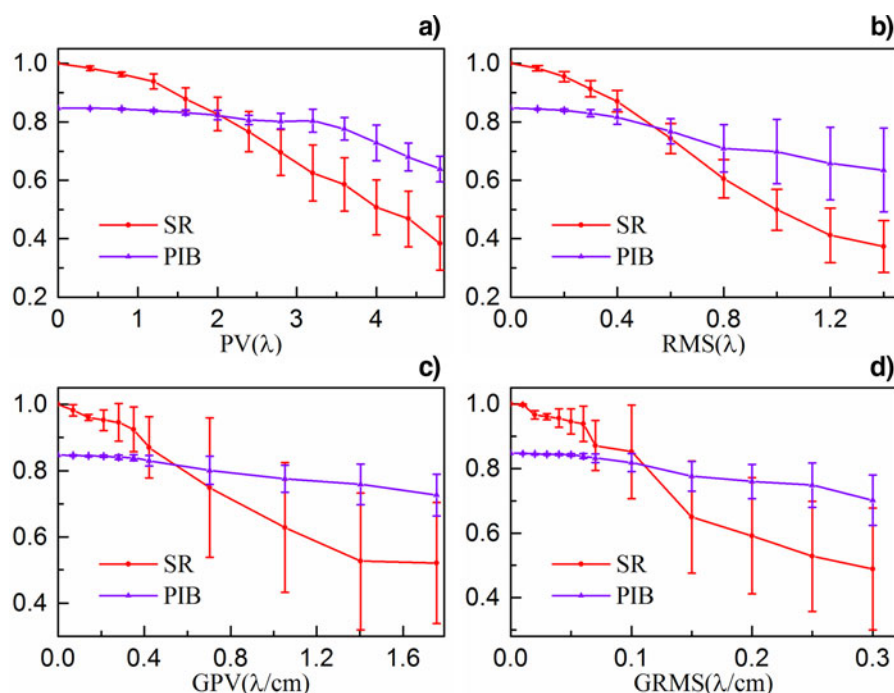


Fig. 3. Relationships between the statistical value of IPWE and the performance of LATG. (a) PV, (b) RMS, (c) GPV, and (d) GRMS.

Table 2. Demands of IPWE parameters for design goals

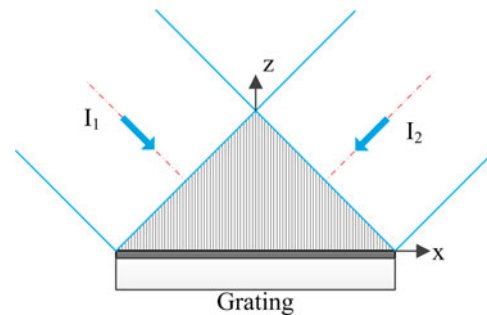
Goals	Demands of IPWE			
	PV(λ)	RMS(λ)	GPV(λ/cm)	GRMS(λ/cm)
SR > 0.9	1.26	0.27	0.22	0.052
PIB > 0.76	3.25	0.49	0.68	0.12

and so on. The latter is induced by wave aberration of holographic exposure when processing the grating. In this section, we will discuss surface deformation and wave aberration in detail, which is useful in choosing appropriate gratings for LATG compressor.

Grating surface deformation

Commercial multi-layer dielectric gratings are available as 0.5-meter-class optical elements with 40–50 mm thicknesses (Reinlein *et al.*, 2016). The surface deformation induced by coating stress exhibits a parabolic shape, the value of deformation in the center is smaller than the edge (Qiao *et al.*, 2015) and deformation quality of $\lambda/5$ to $\lambda/3$ at 1053 nm can be obtained on 0.5-meter-class optics (Reinlein *et al.*, 2016). A finite-element analysis model of the grating is built using the commercial software ANSYS with 45 mm thickness to predict grating deformation. We find that the deformation caused by the tiled mount, which is influenced by grating thickness, and the deformation caused by substrate gravity, which is insensitivity direction of diffraction, can be ignored compared with the deformation caused by coating stress. Therefore, we focus in this paper on the influence of deformation caused by coating stress.

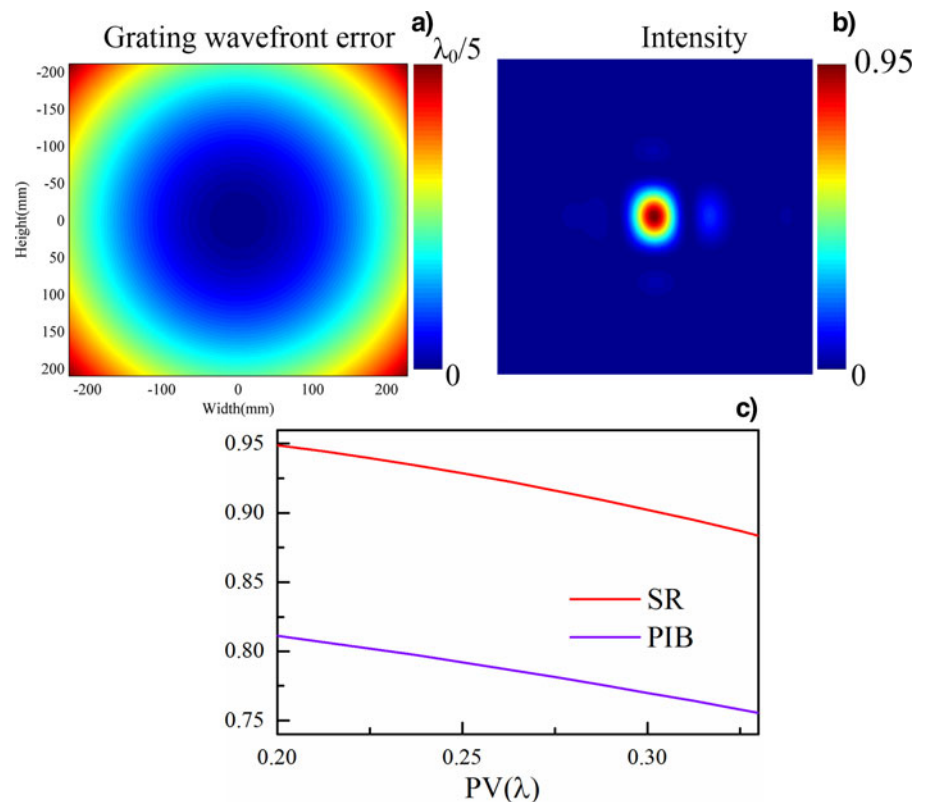
A parabolic shape is introduced to each grating in the computer model to calculate the influence of coating stress, as

**Fig. 5.** Sketch of making a holographic exposure grating.

shown in Figure 4a (the grating wavefront errors are PV = 0.2 λ and RMS = 0.0991 λ). Figure 4b manifests the corresponding far field distribution. It is clear that far-field deteriorates because of the coating stress. We observe that the far field is unsymmetrical caused by the symmetrical wavefront of the grating, and it is the consequences of the light escaping of the grating gap and the aperture limit of the G2. Figure 4c presents the relationships between the SR, PIB, and the PV of grating wavefront error. We can see that the SR and PIB approximate linear decreased with the increase of PV. For this system, the certain value of grating wavefront error caused by coating stress to form a focal spot with SR = 0.9 is about PV = 0.3 λ . In a practical system, if we choose the PV value better than this, the LATG compressor performance could be improved.

Grating wave aberration

Machine-ruling and holographic exposure are two main methods for fabricating a monolithic grating, and the latter gratings are widely used to compress the laser pulse in CPA system. The

**Fig. 4.** (a) Grating wavefront error caused by coating stress, PV = 0.2 λ , RMS = 0.0991 λ . (b) Far-field degradation caused by grating wavefront error. (c) Relationships between the SR, PIB and the PV of grating wavefront error.

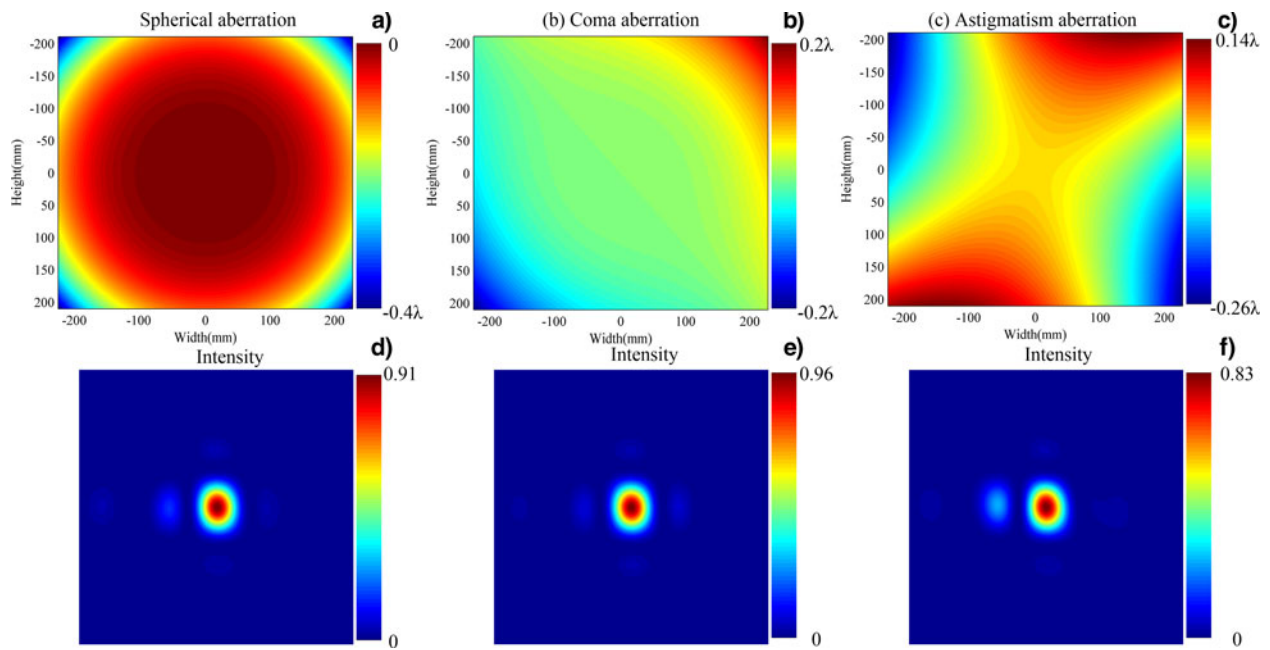


Fig. 6. Far-field for different wave aberration with the same $K = 0.4\lambda$, (a) spherical aberration, (b) coma aberration, and (c) astigmatism aberration. (d), (e), and (f) are the corresponding far field.

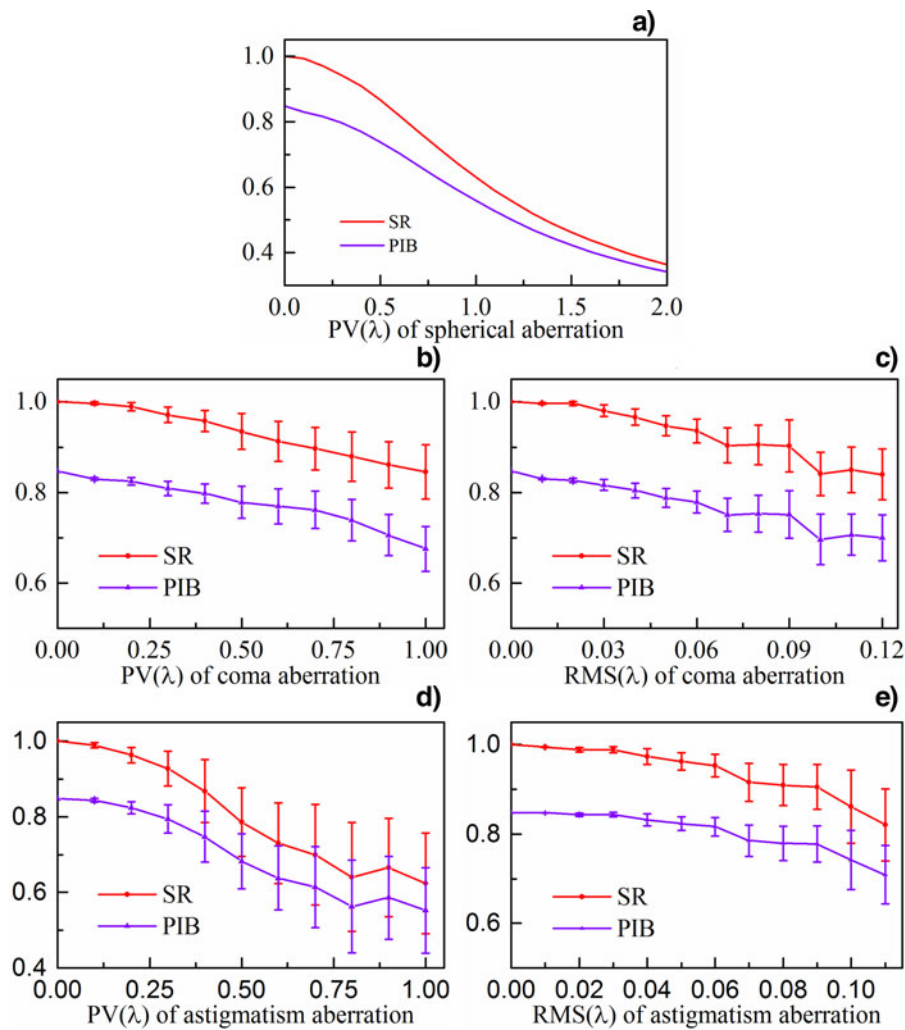


Fig. 7. Relationships between each wavefront aberration and LATG performance. (a) PV of spherical aberration. (b) PV of coma aberration, and (c) RMS of coma aberration. (d) PV of astigmatism aberration, and (e) RMS of astigmatism aberration.

Table 3. Demands of wave aberration for design goals

Goals	Demands of grating wave aberration				
	Spherical PV(λ)	Coma		Astigmatism	
		PV(λ)	RMS(λ)	PV(λ)	RMS(λ)
SR > 0.9	0.42	0.49	0.062	0.27	0.065
PIB > 0.76	0.43	0.45	0.056	0.29	0.067

sketch of making a holographic exposure grating is represented in Figure 5. Between two consecutive exposures, the phase of the exposure beams I_1 and I_2 may have difference caused by the error of exposure system. Assuming the wave aberrations of I_1 and I_2 are $\varphi_1(x, y)$ and $\varphi_2(x, y)$, respectively, then the interference fringes can be expressed as (Shi *et al.*, 2009)

$$\tau(x, y) = C \exp \left\{ ia \cos \left[\frac{2\pi x}{d} + 2\pi\varphi(x, y) \right] \right\} \quad (7)$$

where C and a are constants. d is the grating period. $\varphi(x, y) = \varphi_1(x, y) - \varphi_2(x, y)$ is the wave aberration of grating and will distort the grating grooves.

For the holographic exposure system, the wave aberration can be presented as (Yu, 1996)

$$\varphi(x, y) = K \frac{\eta_0(x, y)}{\max[\eta_0(x, y)] - \min[\eta_0(x, y)]} \quad (8)$$

where K is the PV of the wave aberration. $\eta_0(x, y) = A_1(x^2 + y^2)^2 + A_2y(x^2 + y^2) + A_3x(x^2 + y^2) + A_4y^2 + A_5x^2 + A_6xy$, A_1 is the coefficient of spherical aberration, A_2 and A_3 are the coefficients of coma aberration, A_4 , A_5 , and A_6 are the coefficients of astigmatism aberration.

Supposing the gratings G11, G12, G21, and G22 are products of the same batch, that is the wave aberration of four gratings is the same. To investigate the effects of different aberrations, we introduce the same K value to all kinds of aberrations. The wave aberrations and the corresponding far-field results are exhibited in Figure 6, $K = 0.4 \lambda$. We find that the effects of different wave aberrations with the same K value on the performance of LATG are different, and the effects of spherical aberration and astigmatism aberration are greater than coma aberration in this case. Far fields caused by symmetrical spherical aberration and astigmatism aberration also are unsymmetrical.

To estimate the tolerance of each wave aberration and agreement with laboratory conditions, we reuse the Monte Carlo method and introduce the random wave aberration from Eq. (8) many times at each value and the relationships between parameters of wave aberrations and LATG performance are indicated in Figure 7. Since the parameters of wave aberrations are interrelated from the expression of Eq. (8) and φ_0 , there just list partial results. The relationships between spherical aberration and SR, PIB are represented in Figure 7a, the relationships between coma aberration and SR, PIB are illustrated in Figure 7b and 7c, and the influences of astigmatism aberration are shown in Figure 7d and 7e. The changing trends of these curves are all similar and the influences of coma and astigmatism are likely with the influence of IPWE. The wave aberration affects the LATG performance considerably. The corresponding requirements of different wave aberration for a series of goals are given in Table 3.

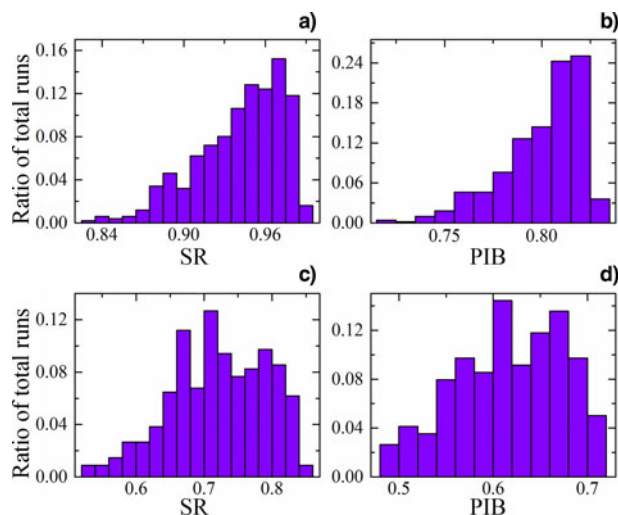


Fig. 8. (a) and (b) Histograms of SR and PIB with tiling errors without wavefront errors. (c) and (d) Histograms of SR and PIB with tiling errors and wavefront errors.

Discussion

The studies of aforementioned in this paper are based on spatial performance. However, the perfect focal spot in space does not mean the perfect pulse in time. We use its full width at half of its maximum value (FWHM) to characterize the spatially integrated to examine the tolerances. For an ideal system, the FWHM is 543 fs (transform limit). We introduce the wavefront errors within tolerance limits mentioned in the previous, we find that the FWHM increases with the increase of all wavefront errors, the effect of grating deformation on pulse broadening is greater than other wavefront errors, and the FWHM is 591 fs when the PV of grating deformation is 0.3λ . The FWHM remains close to its transform-limited value even the worst condition, so the wavefront error tolerances satisfy the requirements in temporal performance.

Moreover, the error tolerances for different wavefront errors are analyzed based on single factor condition. Nevertheless, the far field is a synthetical result of all influence factors, so we introduce tiling errors and wavefront errors simultaneously to predict the performance of LATG compressor accurately. In our model, the accuracy requirements when SR equivalent to 0.9 for three tiling errors piston, tilt, and tip are 75 nm, $0.51 \mu\text{rad}$, and $0.29 \mu\text{rad}$, respectively. Figure 8 presents the histograms of the far-field performance of 500 randomly realized LATG compressors for two cases: With tiling errors but without wavefront error, and with both tiling errors and wavefront errors. In the latter case, we assume the wavefront errors are better controlled, the RMS of IPWE is within 0.27λ , the PV of grating deformation is 0.25λ , and the specific weight of three wave aberrations are equally and the PV of the wave aberration is 0.4λ . From this simulation, the performance of LATG for two cases can be predicted statistically. For the former case, the LATG compressor almost satisfies the application requirement. For the latter case, we observe that the far field degrades considerably compared with the former one, that is even each wavefront error is controlled within the tolerance, the LATG performance still needs correction elements (such as a deformable mirror) to correct the wavefront distortion to satisfy the requirement.

Conclusion

In conclusion, the IPWE, coating stress, and wave aberration, which can affect the wavefront distortion of output laser pulse for LATG compressor, are investigated. A model is built to describe the TG compressor. We have discussed how the different wavefront errors affect the far field distribution and calculated the error tolerances by a series of numerical simulations. We find that the far field degrades significantly with the increased of the wavefront errors even if there is no tiling error. The error tolerances (PV) of input wavefront, grating deformation, spherical aberration, coma aberration, and astigmatism aberration when SR equivalent to 0.9 are 1.26λ , 0.3λ , 0.42λ , 0.49λ , and 0.27λ , respectively, and the performance of LATG compressor can be improved if we make wavefront parameters better than these values. For an actual CPA system, it is essential to find a way to correct the wavefront distortion to improve the quality of far-field even though the above wavefront errors are better controlled. All these works are meaningful to choose appropriate gratings and improve the quality of input pulse for constructing the LATG compressor in the future.

Acknowledgment. This work was supported by the National Natural Science Foundation of China (Grant No.61308040).

References

- Blanchot N, Bar E, Behar G, Bellet C, Bigourd D, Boubault F, Chappuis C, Coïc H, Damiensdupont C and Flour O (2010) Experimental demonstration of a synthetic aperture compression scheme for multi-Petawatt high-energy lasers. *Optics Express* **18**, 10088–10097.
- Bonod N and Neaupourt J (2016) Diffraction gratings: From principles to applications in high-intensity lasers. *Advances in Optics and Photonics* **8**, 1–44.
- Bunkenburg J, Kessler TJ, Skulski W and Huang H (2006) Phase-locked control of tiled-grating assemblies for chirped-pulse-amplified lasers using a Mach-Zehnder interferometer. *Optics Letters* **31**, 1561–1563.
- Daiya D, Sharma AK, Joshi AS, Naik PA and Gupta PD (2013) Theoretical and experimental studies on single tiled grating pulse compressor. *Optics Communications* **309**, 15–20.
- Daiya D, Patidar R, Sharma J, Joshi A, Naik P and Gupta P (2017) Optical design and studies of a tiled single grating pulse compressor for enhanced parametric space and compensation of tiling errors. *Optics Communications* **389**, 165–169.
- Dorrer C, Consentino A, Irwin D, Qiao J and Zuegel JD (2015) OPCPA front end and contrast optimization for the OMEGA EP kilojoule, picosecond laser. *Journal of Optics*. **17**, 094007.
- Fang Z, Xia L, Chen G, Huang Y, Xu D and Tan M (2014) Vision-based alignment control for grating tiling in Petawatt-class laser system. *IEEE Transactions on Instrumentation and Measurement* **63**, 1628–1638.
- Habara H, Xu G, Jitsuno T, Kodama R, Suzuki K, Sawai K, Kondo K, Miyanaga N, Tanaka KA and Mima K (2010) Pulse compression and beam focusing with segmented diffraction gratings in a high-power chirped-pulse amplification glass laser system. *Optics Letters* **35**, 1783–1785.
- Hornung M, Bödefeld R, Kessler A, Hein J and Kaluza MC (2010) Spectrally resolved and phase-sensitive far-field measurement for the coherent addition of laser pulses in a tiled grating compressor. *Optics Letters* **35**, 2073–2075.
- Jahns J, Turunen J and Wyrowski F (1999) Diffractive optics for industrial and commercial applications. *Laser and Part Beams* **7**, 139–141.
- Kessler TJ, Bunkenburg J, Huang H, Kozlov and Meyerhofer DD (2004) Demonstration of coherent addition of multiple gratings for high-energy chirped-pulse-amplified lasers. *Optics Letters* **29**, 635–637.
- Kruschwitz BE, Jungquist R, Qiao J, Abbey S, Dean SE, Maywar DN, Moore MD, Waxer LJ and Wilson ME (2006) Large-aperture deformable mirror correction of tiled-grating wavefront error. *Journal De Physique IV* **133**, 645–648.
- Lawson JK, Auerbach JM and English RE (1999) NIF optical specifications—the importance of the RMS gradient. *SPIE* **3492**, 336–343.
- Li ZY, Xu G, Wang T and Dai YP (2010) Object-image-grating self-tiling to achieve and maintain stable, near-ideal tiled grating conditions. *Optics Letters* **35**, 2206–2208.
- Mourou G and Tajima T (2011) The extreme light infrastructure: Optics' next horizon. *Optics and Photonics News* **22**, 47–51.
- Oliver JB, Keck J, Rigatti AL and Kosc TZ (2005) Thin-film design for multilayer diffraction gratings. *SPIE* **5991**, 59911A.
- Qiao J, Kalb A, Guardalben MJ, King G, Canning D and Kelly JH (2007) Large-aperture grating tiling by interferometry for petawatt chirped-pulse-amplification systems. *Optics Express* **15**, 9562–9574.
- Qiao J, Papa J and Liu X (2015) Spatio-temporal modeling and optimization of a deformable-grating compressor for short high-energy laser pulses. *Optics Express* **23**, 25923–25934.
- Reinlein C, Damm C, Lange N, Kamm A, Mohaupt M, Brady A, Goy M, Leonhard N, Eberhardt R and Zeitner U (2016) Temporally-stable active precision mount for large optics. *Optics Express* **24**, 13527–13541.
- Sharma A, Joshi A, Naik P and Gupta P (2017) Active phase locking of a tiled two-grating assembly for high-energy laser pulse compression using simultaneous controls from far-field profiles and interferometry. *Applied Physics B*. **123**, 117.
- Shi L, Zeng LJ and Li LF (2009) Fabrication of optical mosaic gratings with phase and attitude adjustments employing latent fringes and a red-wavelength dual-beam interferometer. *Optics Express* **17**, 21530–21543.
- Smith DJ, Mikami T and Jitsuno T (2008) Low stress ion-assisted coatings on fused silica substrates for large aperture laser pulse compression gratings. *SPIE* **7132**, 71320E.
- Yakovlev IV (2014) Stretchers and compressors for ultra-high power laser systems. *Quantum Electronics* **44**, 393–414.
- Yu MW (1996) *Optical Holography and its Application*. Beijing: Beijing Institute of Technology Press.
- Zhang T, Yonemura M and Kato Y (1998) An array-grating compressor for high-power chirped-pulse amplification lasers. *Optics Communications* **145**, 367–376.
- Zuo Y, Wei XF, Wang X, Zhu QH, Ren R, Huang Z, Liu H and Ying C (2007) Eliminating the longitudinal piston error between tiled gratings by angle tuning. *Optics Letters* **32**, 280–282.